INORGANIC CHEMISTRY
FRONTIERS

RESEARCH ARTICLE

View Article Online
View Journal

Cite this: DOI: 10.1039/d6qi00660d

Redox-responsive Fe(II)/Fe(III) MRI probes with pentadentate or hexadentate macrocyclic ligands

Deepak Krishnan Balaji, [a] Joseph A. Spernyak, [b] Matthew R. Crawley [a] and Janet R. Morrow *[a]

Fe(II) complexes of TACN (1,4,7-triazacyclononane) containing two 6-methyl-2-picolyl pendant groups are studied as redox-responsive agents for monitoring peroxide produced in inflammation. One Fe(II) complex has a pentadentate ligand with a sixth coordination site for binding water as confirmed by X-ray crystallography ($[Fe^{II}(MPB)(CF_3SO_3)](CF_3SO_3)$) and by ^{17}O NMR studies in solution. The other complex is formed with a hexadentate ligand ($Fe^{II}(MPH)$) and also has an inner-sphere water ligand in solution as shown by variable temperature ^{17}O NMR studies. $Fe^{II}(MPB)$ is inert towards oxidation under ambient levels of O_2 in aqueous solution at pH 7.4 over 24 hours whereas $Fe^{II}(MPH)$ is resistant to oxidation over 4 hours. $Fe^{II}(MPB)$ oxidizes rapidly (≤3 min) upon addition of one equivalent of peroxide or in the presence of 0.1 U mL^{-1} glucose oxidase (GOX). With one equivalent of peroxide in buffered solutions, the major product is $Fe^{III}(MPB)$, most likely as a buffer or hydroxide complex, but with a 10-fold excess of peroxide, a Fe(III) phenolate complex is produced as supported by electronic absorbance spectroscopy and analysis of products by high resolution mass spectrometry. The r_1 relaxivity for the $Fe^{III}(MPB)$ (r_1 = 0.71 mM^{-1} s^{-1}) is increased by 14-fold over the Fe^{II} complex at 1.4 T, 34 °C and pH 7.4. Oxidation of $Fe^{II}(MPH)$ by addition of one equivalent of peroxide or by GOX is complete within a few minutes and produces a 7-fold increase in relaxivity (r_1 = 0.58 $mM^{-1}s^{-1}$) . Changes in relaxivity are reversed by addition of ascorbate. $Fe^{II}(MPB)$ is one of the first reported examples of a Fe(II) macrocyclic MRI probe that is unreactive to O_2 but reacts rapidly with micromolar concentrations of peroxide for increased selectivity in monitoring inflammation.

Received 31st March 2026,
Accepted 3rd May 2026

DOI: 10.1039/d6qi00660d

rsc.li/frontiers-inorganic

Introduction

Contrast agents are essential tools in modern magnetic resonance imaging (MRI) diagnostic protocols.[1] Clinically used gadolinium-based MRI contrast agents are administered intravenously and extravasate into tissue in a non-specific manner to produce a dynamically monitored signal for the visualization of pathophysiological states and anatomic details for tumor detection, angiography, blood–brain barrier evaluation and organ perfusion.[2] In molecular MRI, contrast agents or probes provide further information towards diagnosis in the presence of biochemical markers or specific physiological environments.[3] Such probes may either be attached to a targeting agent or contain a responsive element that leads to activation of the probe under aberrant physiological conditions.[3] Such responsive probes would facilitate mapping tissue changes that are a result of molecular processes characteristic of disease states and would add to the information normally gained from a contrast agent. Responsive or activatable MRI probes have been reported for wide-ranging applications such as enzyme reactions,[4,5] pH changes,[3,4] redox status[6–8] or metal ion concentrations.[9,10]

One sought-after type of activatable MRI probe responds to the oxidizing conditions found in inflammation[7,8,11] as postulated to be important in many disease states.[12–15] For example, the capability to image reactive oxygen species (ROS) may enable discrimination of inflammation *versus* tumor growth during cancer treatment as a biochemical signature.[14,16,17] Of the ROS, peroxide is the most likely biochemical marker to react with an MRI probe as it is present in micromolar concentrations in the extracellular environment[18] and is generated by myeloid immune cells that are recruited to the site of inflammation.[19] Other ROS such as hydroxyl or superoxide radicals are likely to be too reactive for registration by probes under physiological conditions.[20]

Probes based on Gd(III) T_1 agents were among the earliest examples of redox-responsive probes. These Gd(III) complexes contained ligands that react under oxidizing conditions or with thiol-reactive ligands to give increased signal.[21,22] More

[a]Department of Chemistry, University at Buffalo, The State University of New York, Amherst, New York 14260, USA. E-mail: Jmorrow@buffalo.edu
[b]Department of Cell Stress Biology, Roswell Park Comprehensive Cancer Center, Buffalo, New York 14263, USA

recently, redox-activated MRI probes containing Gd(III) complexes tagged with groups to produce signal by ^{19}F NMR/MRI have been reported.[23] An alternative approach is to use a redox-active metal that switches oxidation states. These are generally transition metal probes[6,8,9,24] or certain lanthanides such as Eu(II)/Eu(III) complexes.[25–27] The tunability of the redox potential of the metal center through coordination chemistry makes them ideal for development as responsive MRI probes. The effect of the probe on water proton resonances[6–8] or on ^{19}F NMR/MRI signal of fluorine-containing tags can be monitored.[28,29] Switchable paramagnetic chemical exchange saturation transfer (paraCEST) probes have also been reported.[30,31]

Of the early transition metal ions, iron probes are of interest to capitalize on the abundance of iron in the body and the tunable redox range of the Fe(II)/Fe(III) couple in coordination complexes.[8,32] There are two common spin states for each member of the Fe(II)/Fe(III) redox pair. High-spin Fe(II) is a shift agent for frequency-encoded methods such as paramagnetic shift or paraCEST agents and is not an effective relaxation agent,[8,33,34] whereas low spin Fe(II) is diamagnetic and thus MRI silent. High-spin Fe(III) is a T_1 agent[32,35,36] whereas low spin Fe(III) is a paramagnetic shift agent.[37] The most commonly-studied redox pair for MRI applications is Fe(II) (high-spin or low spin) to high-spin Fe(III) complexes.[6,8] For this responsive pair, the divalent Fe(II) is the form of probe that is injected and, upon oxidation, gives rise to increased signal in T_1 weighted imaging.[38] One of the major challenges in this endeavor is to obtain complexes that oxidize in the presence of peroxide and not O_2, given that O_2 is present in blood and organs. Thus, it is desirable that the redox potential for the Fe(II)/Fe(III) couple is positive *versus* NHE (>200 mV) to favor the Fe(II) state under normal physiological conditions, but to produce Fe(III) under oxidizing conditions of inflammation. Of the handful of reported redox-activated iron agents, macrocyclic complexes are activated only at high concentrations of peroxide (10–100 mM) that are not biologically relevant[39–41] and recent examples of closed coordination complexes with multiple metal centers also require excess millimolar concentrations of peroxide.[42,43] In contrast, iron probes containing polyaminocarboxylate pendants and an available coordination site react readily with enzymatically generated peroxide.[38,44] These linear polyaminocarboxylate-based probes have been studied *in vivo* to map inflammatory processes.[44–47] However, the Fe(II) form of the probes oxidizes slowly in the presence of O_2 over several hours.

Here we report our efforts to prepare Fe(II)/Fe(III) redox activated probes that do not react readily with O_2 in aerated solutions but react rapidly with micromolar amounts of peroxide. The key probe is an Fe(II) complex with a high redox potential (680 mV *versus* NHE) and an available coordination site for reacting with peroxide in the first step of oxidation. The iron complexes studied here (Scheme 1) are inspired by peroxide oxidation studies of Fe(II) complexes containing five nitrogen donor atoms, based mostly on linear[48,49] and some macrocyclic chelates.[50]

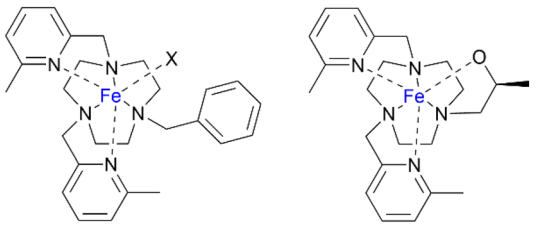

Fe^{II}(MPB) Fe^{III}(MPB) Fe^{II}(MPH) Fe^{III}(MPH)

Scheme 1 Iron complexes studied as redox probes with general labels designating all species in solution. X = OH_2, OH, buffer, or peroxide.

Results and discussion

Synthesis and characterization of ligands and Fe(II) complexes

Two complexes were prepared with the goal of examining the effect of macrocyclic ligands with different denticity on the oxidation and reduction of an activatable MRI probe. The MPB ligand is pentadentate and forms a Fe(II) complex with an available coordination site for a sixth ligand. The MPH ligand is hexadentate and preserves two pendant 6-methyl-2-picolyl (methylpyridine) groups but has a third pendant with an oxygen donor to tune the redox potential to more negative values compared to Fe(II) complexes with all nitrogen donors.[51] The methyl group on the pyridine pendant serves to maintain a high-spin state for Fe(II)[51] and Fe(III). Analogous iron complexes of TACN with 2-picolyl pendants that lack the methyl group adjacent to the nitrogen donor give low or intermediate spin-states for Fe(II) or Fe(III) complexes.[52–54] Our goal is to produce increased signal from a low relaxivity probe containing high-spin Fe(II) to a higher relaxivity probe containing high-spin Fe(III).[38]

The MPB ligand was prepared from benzyl TACN by addition of 6-methyl-2-picolyl pendants by reductive amination methods.[51,55] To prepare MPH, the benzyl group of MPB was removed by catalytic hydrogenation followed by alkylation with S-propylene oxide. The Fe(II) complexes were synthesized upon addition of $Fe(CF_3SO_3)_2$ and isolated as the triflate salts. Both complexes are water soluble up to 5 mM at neutral pH and had effective magnetic moments (Fig. S2 and S3) of 5.3 and 5.1, respectively that are consistent with high-spin Fe(II) complexes.

X-ray crystallography studies showed a hexacoordinate $[Fe^{II}(MPB)(CF_3SO_3)](CF_3SO_3)$ complex with three bound nitrogens of the TACN macrocycle, two 6-methyl-2-picolyl nitrogens and the sixth coordination site occupied by triflate counterion (Fig. 1). The $[Fe^{II}(MPB)(CF_3SO_3)](CF_3SO_3)$ complex crystallizes in the triclinic crystal system and the centrosymmetric space group $P\bar{1}$. The twist angle (θ) of the complex was determined as the dihedral angle formed between the centroids of two mean planes and two atoms, each selected from one of the planes. One plane was defined by the two coordinated pyridyl nitrogen atoms and the bound oxygen of the triflate, while the

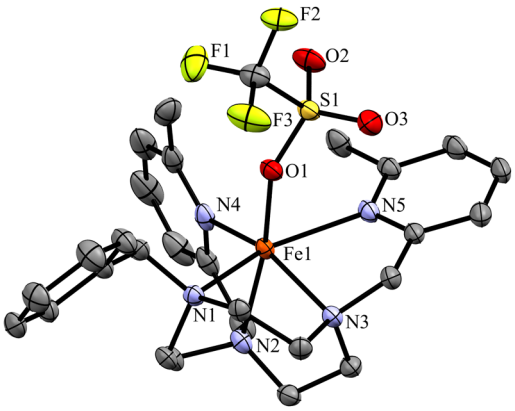

Fig. 1 Molecular structure of $[Fe^{II}(MPB)(CF_3SO_3)]^+$ cation – Δ(λλλ) as ORTEP diagram (hydrogen, counter anion and solvent molecule omitted for clarity).

other was defined by the three coordinated nitrogen atoms of the macrocycle.

Based on the twist angle (35.7°) and direction (clockwise) of rotation of mean planes, the overall chirality of the complex is determined as Δ and based on the helicity of the macrocyclic backbone the chirality is determined as λλλ. The asymmetric unit of $[Fe^{II}(MPB)(CF_3SO_3)]^+$ contains one full isomer Δ(λλλ) of this complex (Fig. 1). Given that the space group is centrosymmetric, the crystal structure also contains the inversion isomer Λ(δδδ) (Fig. S1). Additionally, the twist angle is consistent with a distorted octahedral geometry of the complex.

The ^{1}H NMR spectrum (Fig. 2B) of Fe^{II}(MPB) shows 26 distinct proton resonances, consistent with a single diastereomeric form in solution. The chemical shifts of the proton resonances range from 193 ppm to −67 ppm.

The narrow and intense resonance at −39 ppm is assigned as one of the methyl resonances of a pyridine pendant based on its integration and T_2 value (1.2 ms). The second methyl resonance is likely at 29 ppm as it has a similar integration value and T_2 value (2.3 ms). The ^{1}H NMR spectrum (Fig. 2A) of Fe^{II}(MPH) shows 26 distinct proton resonances, consistent with a single diastereomeric form in solution. The proton chemical shifts span a slightly larger range from 230 ppm to −60 ppm. The methyl groups are assigned by their integration and T_2 values (0.8 ms) and have chemical shifts (37 ppm and −38 ppm) similar to those of Fe^{II}(MPB).

The Fe(II) complexes exhibit electronic absorbance bands at 360 nm that are assigned to MLCT bands which are lacking in the spectrum of the ligand alone (Fig. S6). Monitoring these bands upon incubation shows that both complexes are inert over several hours in the presence of 25 mM carbonate and 0.5 mM phosphate at pH 7.4 and 37 °C (Fig. S7 & S9). The complexes remained intact upon incubation with an equivalent of Zn(II) over several hours (Fig. S8 & S10). In addition, the oxidation of the two complexes was monitored by UV-vis spectroscopy at pH 7.4 in buffered aerated solutions. Fe^{II}(MPB) showed a negligible change in absorbance at 320 nm over 24 hours in the presence of ambient concentrations of oxygen in buffered solutions at neutral pH (Fig. 3). In contrast, Fe^{II}(MPH) showed a gradual change in absorbance that was attributed to oxidation with up to 20% oxidation by 24 hours.

Solution speciation of the Fe(II) complexes was studied by monitoring electronic absorbance spectra as a function of pH. A pH titration of Fe^{II}(MPB) showed the disappearance of the

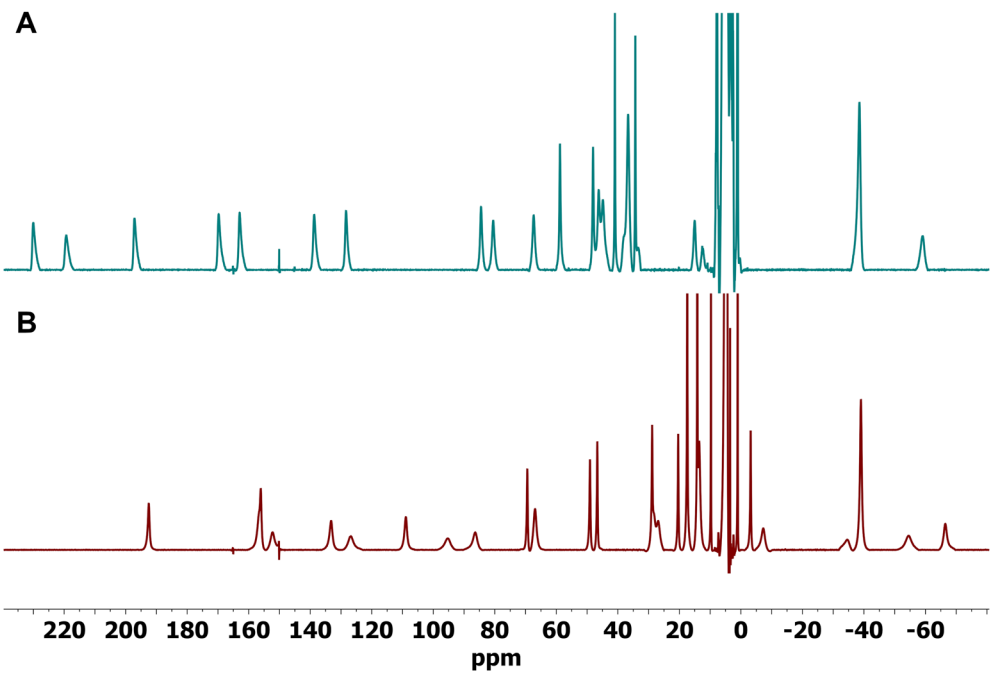

Fig. 2 ^{1}H NMR spectra of (A) Fe^{II}(MPH) and (B) Fe^{II}(MPB) complexes in D_2O.

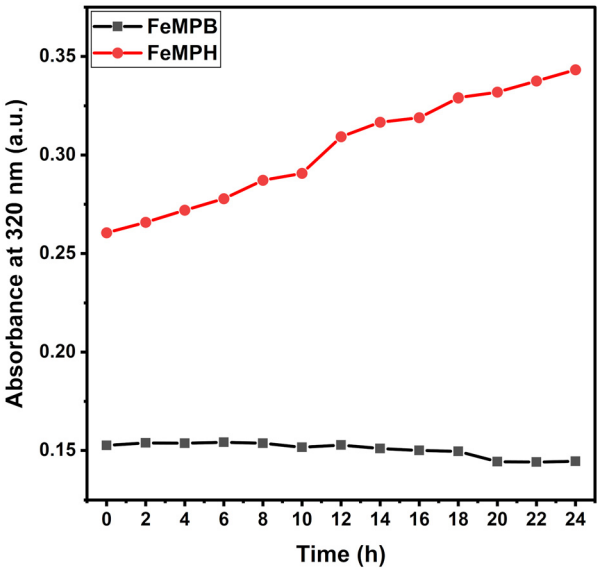

Fig. 3 Inertness of Fe(II) complexes to oxidation by oxygen monitored by UV-Vis absorbance at 320 nm. Conditions: 0.20 mM complex, 20 mM HEPES pH 7.4.

peak at 360 nm and an increase in a new absorbance peak at 425 nm as the pH was increased from 4.5 to 11. A plot of the peak intensity at 360 nm as a function of pH (Fig. 4B & Fig. S11) gave a pK_a value of 9.8 whereas a plot of the peak intensity at 400 nm as a function of pH gave a similar pK_a value of 9.9. These data suggest that the Fe^{II}(MPB)(OH_2) complex deprotonates, but only at high pH. The group that deprotonates with this high pK_a is most likely the Fe(II) bound water to form the Fe^{II}(MPB)(OH) complex. An analogous pH titration to determine the pK_a of the hydroxyl of Fe^{II}(MPH) was not feasible as the complex oxidized to the Fe(III) form at basic pH values. However, the cyclic voltammetry of the complex in water as a function of pH as discussed below suggests that the pK_a is ≈9 for the Fe^{II}(MPH) complex, most likely due to deprotonation of the hydroxyl group. A pH titration of the oxidized complex, Fe^{III}(MPH), showed changes in the UV-vis bands that were consistent with a pK_a of close to 6. This pK_a value is similar to that of other Fe(III) complexes with hydroxyl groups,[56] suggesting deprotonation of this pendant (Fig. S12 & 13).

Variable-temperature ^{17}O NMR spectra recorded over the temperature range 25 to 75 °C are presented in (Fig. 4C) and in SI (Fig. S16). In this temperature range at pH 5 and 7.45 mM, the Fe^{II}(MPB) complex produces broadening and a paramagnetically induced shift of the bulk water ^{17}O resonance, consistent with behavior expected for complexes with an inner-sphere bound water molecule. The resonance is broader at lower temperature and sharpens as the temperature increases. A plot of $\ln 1/T_{2R}$ *versus* temperature (Fig. 4D) showed the upward curve indicating the temperature dependence of the transverse relaxivity is dominated by the changes in the water exchange rate.[57] A transition from the slow-exchange regime at low temperatures to the fast exchange regime at higher temperatures relative to the NMR timescale was observed. These data were fit to Swift Connick equations to determine the activation parameters (Table S4) including enthalpy, entropy and an exchange rate constant of 2.4×10^6 s^{-1} at 25 °C. Plots of the reduced chemical shift as a function of temperature (Fig. S14) gave k_{ex} values about 3-fold larger and global fitting efforts (Fig. S15) gave relatively poor fits. We attribute these discrepancies to relatively low concentrations of complex (7.45 mM) that were used due to solubility restrictions whereas these studies are typically carried out with 20–40 mM complex.[58] Variable temperature ^{17}O NMR studies with Fe^{II}(MPH) at pH 4.0 (Fig. S16 and S17) also were consistent with an inner-sphere water with a k_{ex} of 3.1×10^6 s^{-1}. An inner-sphere water in this complex may result from the formation of a seven-coordinate complex or by displacement of the hydroxypropyl pendant as the temperature is raised in the ^{17}O NMR experiment. At 25 °C, we propose that the hydroxypropyl pendant is bound based on the ^1H NMR spectrum and electrochemical properties (see below) which differ from those of Fe^{II}(MPB). If the hydroxypropyl pendant was not bound, the ^1H NMR and the redox potential of Fe^{II}(MPH) would be expected to be very similar to that of Fe^{II}(MPB). The k_{ex} rate constants for water exchange in Fe^{II}(MPB) and Fe^{II}(MPH) are similar to those reported for polyaminocarboxylate complexes of Fe(II) which range from 1.1 to 5.5×10^6 s^{-1}.[58–60]

Cyclic voltammetry measurements of the two Fe(II) complexes in water were studied at neutral pH (Fig. 5) and then at several different pH values (Fig. 5 & S19). At pH 7.6, both Fe^{II}(MPB) and Fe^{II}(MPH) have quasi-reversible cyclic voltammetry waves with $E_{1/2}$ of 680 mV and 490 mV, respectively. For Fe(MPB), the wave was consistent with an electrochemically-reversible and chemically-irreversible (E_rC_i) mechanism, in which a quasi-reversible electron transfer step is followed by an irreversible homogeneous chemical reaction of the electrochemically generated product.[61] The Fe^{II}(MPB)(H_2O) complex undergoes one-electron oxidation to give the Fe^{III}(MPB)(H_2O) product. The peak currents associated with this process increase linearly with the square root of the scan rate (Fig. S20), indicating that mass transport is governed by diffusion control as shown by fitting to the Randles–Sevcik equation. The wave with a redox potential of 675 ± 25 mV *versus* NHE and the peak separation between oxidation and reduction waves is substantially larger than the 59 mV expected for a Nernstian one-electron couple and increases systematically with scan rate, consistent with a quasi-reversible redox event.

The pH dependence of the cyclic voltammograms was studied to gain insight into speciation of the two complexes. For Fe(MPB), the wave remained virtually unchanged from pH 6 to 7.6, except for the new reduction peak that appears after the initially observed reduction peak. The 1st reduction (cathodic) peak current is consistently smaller in magnitude than the corresponding oxidation (anodic) peak current with current ratio I_{pc}/I_{pa} of 0.53. This current ratio increases at higher scan rates, which is characteristic of an E_rC_i mechanism. The first oxidation product Fe^{III}(MPB)(H_2O), undergoes

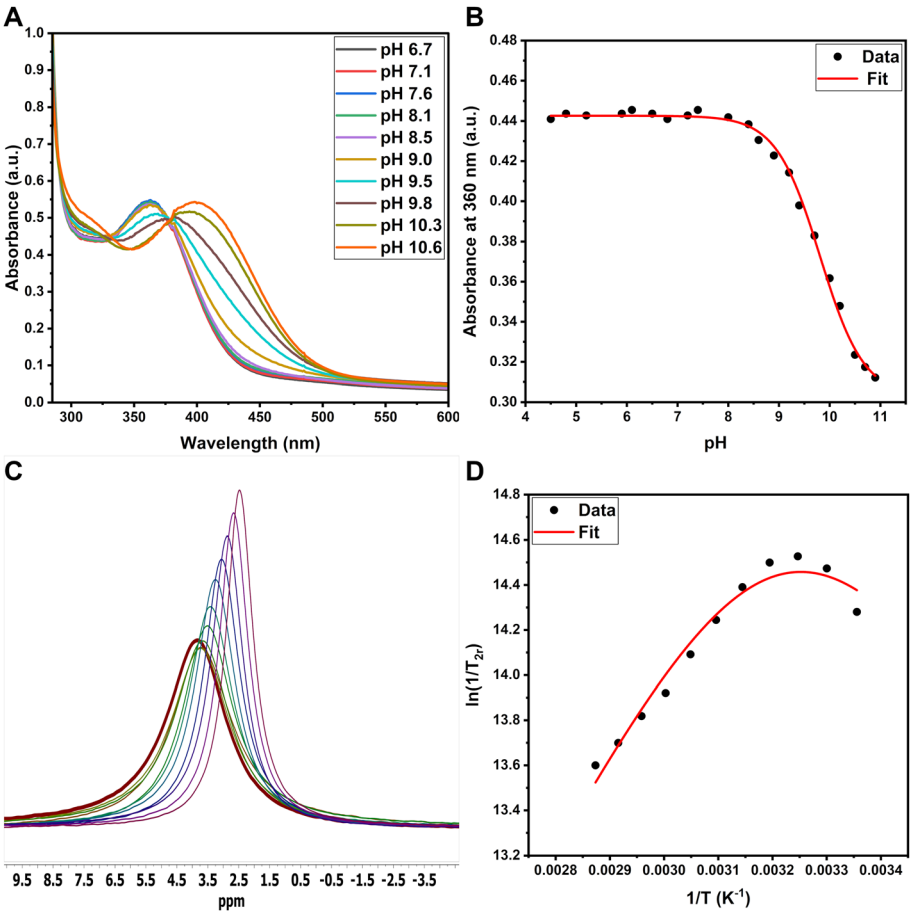

Fig. 4 (A) Electronic spectra and (B) fit of absorbance changes at 360 nm for pH titration of Fe^{II}(MPB) to give a pK_a of 9.8. (C) Variable temperature ^{17}O NMR spectroscopy at pH 5 and (D) reduced transverse relaxation rates in solutions of Fe^{II}(MPB) fit to Swift Connick equations.

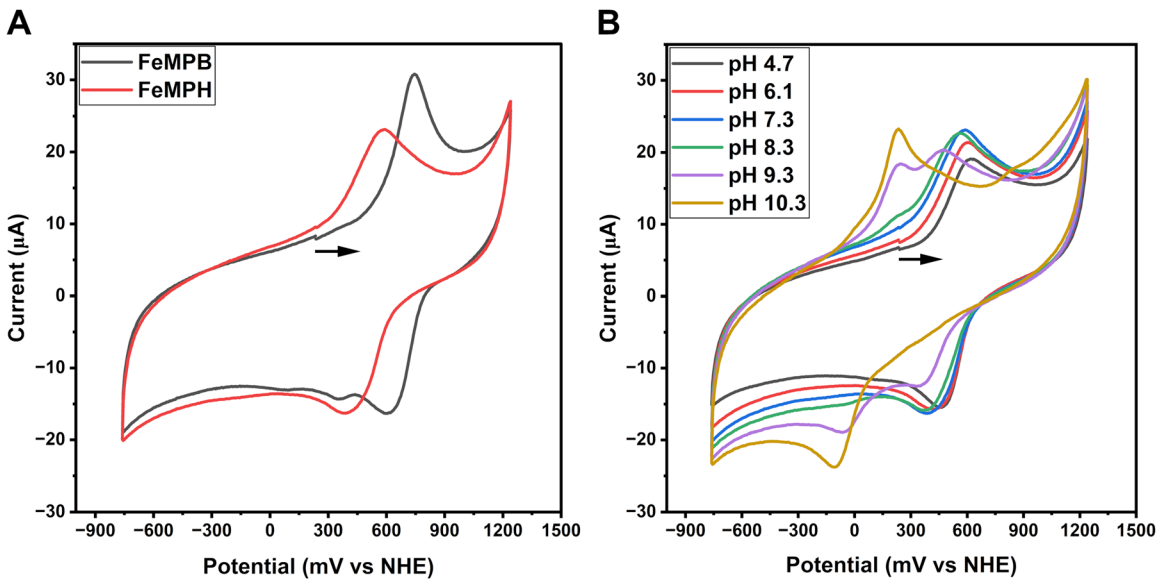

Fig. 5 Cyclic voltammograms of complexes in water at neutral pH (A) and variable pH cyclic voltammogram (B) of Fe^{II}(MPH) complex in water. Conditions: 2 mM complex, 1 M KCl as electrolyte, 100 mV s^{-1} scan speed, (A) pH 7.6 for Fe^{II}(MPB) and pH 7.3 for Fe^{II}(MPH).

deprotonation of bound water to give a hydroxide complex, Fe^{III}(MPB)(OH), which is reduced to form Fe^{II}(MPB)(OH), alongside the major reduction product Fe^{II}(MPB)(H_2O). Fe^{II}(MPH) also shows an E_rC_i type mechanism (Fig. 5B & S21) with quasi-reversible wave at $E_{1/2}$ = 542 mV *versus* NHE at pH 4.7 which shifts slightly to 490 mV at neutral pH. A new wave at lower potential appears by pH 9.3 and continues to grow in at pH 10.3. This quasi-reversible wave is assigned to the deprotonated hydroxypropyl species (Fe(MPH-H+)). The lowered value is consistent with stabilization of the Fe(III) oxidation state by the anionic alkoxide pendant.[56]

Studies at low concentrations of peroxide

Reports of redox-responsive iron probes focus on the effect of oxidants or reductants on the MRI signal and kinetics of oxidation or reduction[38,39,44] yet further characterization of products would be beneficial.[40,41] Here we study the oxidation process and refer to the rich literature on reactions of Fe(II) with peroxide.[48,49,62,63] Many studies of the species formed upon addition of peroxide to Fe(II) complexes are done in methanol or acetonitrile, but there are limited studies in aqueous solution.

The oxidation of Fe^{II}(MPB) and Fe^{II}(MPH) by peroxide was initially studied by electronic absorption spectroscopy. For both complexes, the rate of oxidation with one equivalent of peroxide at neutral pH in buffered solutions was too rapid to be measured by conventional methods (<3 minutes). Under these conditions, the change in absorbance signifying oxidation to Fe(III) was a new absorbance band at 320 nm for Fe^{III}(MPB) (Fig. S24 & S25) and at 300 nm for Fe^{III}(MPH). Complete oxidation of the complexes was observed with one equivalent of peroxide in solutions containing 200 μM complex, concentrations that are relevant for contrast agents[1] and peroxide in the blood stream.[64]

The kinetics of oxidation of Fe^{II}(MPB) and Fe^{II}(MPH) by the enzyme glucose oxidase (GOX) was studied next. GOX produces a steady stream of peroxide in the presence of oxygen and glucose, making it feasible to measure the rate constant for oxidation. As shown in Fig. 6A & S26, both complexes oxidized rapidly in the presence of 0.1 units per mL of enzyme and the reaction rate constant was proportional to the amount of GOX added to solutions (Fig. 6). The initial rates for Fe^{II}(MPB) and Fe^{II}(MPH) with 0.1 units per mL of GOX were 1.5×10^{-4} mM s^{-1} and 2.6×10^{-4} mM s^{-1}, respectively, suggesting slightly higher reactivity for Fe^{II}(MPH), consistent with its lower redox potential. Interestingly, oxidation of the complexes by GOX could be monitored until completion and the data could be fit to an exponential decay curve for a pseudo-first order process due to the large amount of peroxide in excess of complex generated by GOX (Fig. S27 and S33). Notably, only the new peaks at 320 and 300 nm were observed upon oxidation of Fe^{II}(MPB) and Fe^{II}(MPH) by GOX, respectively. However, samples of Fe^{II}(MPB) left to stand for a day in the GOX solution showed a new band at 500 nm, consistent with a buildup of peroxide and the formation of a new species produced by hydroxylation of the benzyl group which is discussed in the next section.

To test the reversibility of the probe towards redox processes, Fe^{III}(MPB) and Fe^{III}(MPH) were generated by treatment of the Fe(II) complexes with half an equivalent of peroxide. Subsequently, two equivalents of ascorbate were added to fully regenerate the Fe(II) complexes as shown by UV-vis spectroscopy (Fig. S39 & S40). Notably, the original electronic absorbance spectra of both Fe^{II} complexes were regenerated nearly instantaneously upon addition of ascorbate.[65]

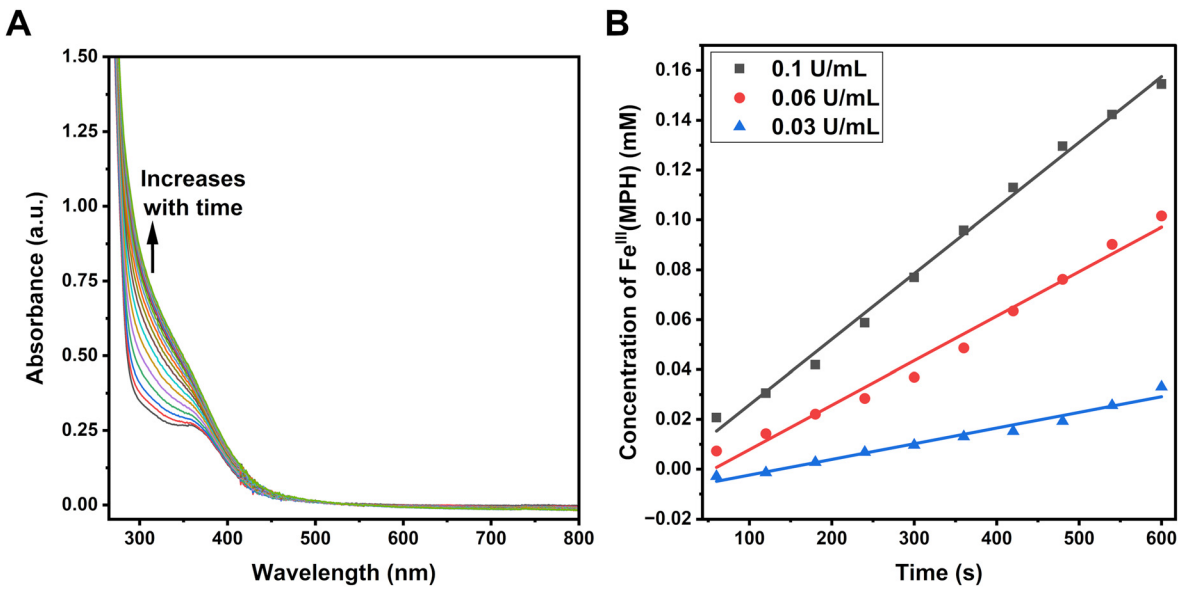

Fig. 6 Electronic spectra to monitor oxidation of Fe^{II}(MPH) with 0.1 U mL^{-1} of glucose oxidase over 48 minutes (A) and oxidation to Fe^{III}(MPH) by different glucose oxidase activity levels monitored *via* absorbance at 300 nm to determine initial rates of reaction (B). Conditions: 0.20 mM complex, 0.1 M NaCl, 100 mM HEPES pH 7.4, 10 mM glucose.

The solution chemistry of the Fe(III) complexes was further studied to probe water interactions and resistance to dissociation. Variable temperature ^{17}O NMR of Fe^{III}(MPB) in aqueous solutions showed very little line broadening of the ^{17}O water resonance (Fig. S41). A plot of line broadening (r_2O) as a function of temperature (Fig. S42) in comparison to Fe^{III}(CDTA) and Fe^{III}(DTPA) reveals that the Fe^{III}(MPB) complex resembles Fe(DTPA), which does not possess inner-sphere water, except for a slight increase in line broadening at higher temperatures. The minimal effect of Fe^{III}(MPB) on the water ^{17}O resonance suggests that the complex does not have an inner-sphere water ligand that exchanges on the NMR time scale. This is attributed to the Fe^{III}(MPB)(X) species with X as a tightly bound water or hydroxide ligand. This result is consistent with other six-coordinate Fe(III) complexes of TACN that exchange inner-sphere water slowly on the NMR time scale.[56,66,67]

Transferrin transchelation of iron was studied for both complexes by monitoring the increase in the absorbance at 465 nm which corresponds to the Fe-transferrin band, with an extinction coefficient of 4950 M^{-1} cm^{-1}. These studies (Fig. S43) revealed that Fe^{III}(MPB) undergoes 30% transchelation to apo-transferrin over five hours with a first order rate constant of 2.2×10^{-3} min^{-1} and half-life of 315 minutes, whereas Fe^{III}(MPH) undergoes less than 10% transchelation to apo-transferrin over five hours. Thus, Fe^{III}(MPH) is highly inert to loss of iron to transferrin, consistent with it being more robust as it contains a hexadentate ligand whereas Fe^{III}(MPB) is inert, but less so. Further aspects of solution chemistry were captured by relaxivity changes over time as discussed below.

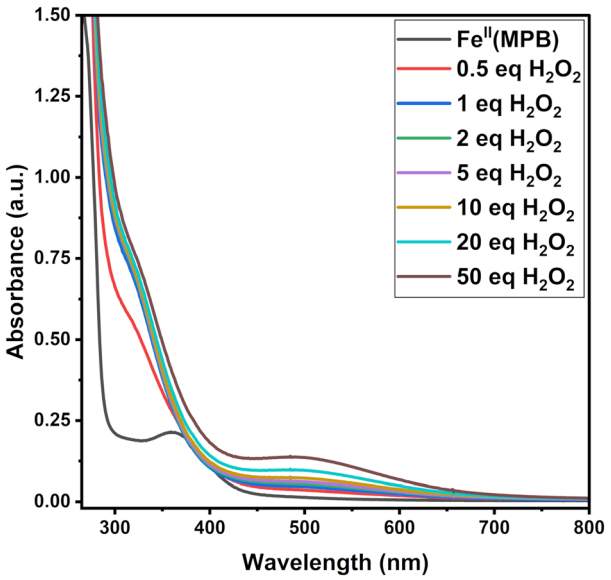

Fig. 7 Electronic spectra tracking the oxidation of Fe^{II}(MPB) with various equivalents of peroxide. Conditions: 0.20 mM complex, 0.10 to 10 mM H_2O_2, 0.1 M NaCl and 20 mM HEPES pH 7.4.

Studies with excess peroxide

Upon addition of an excess of peroxide to Fe^{II}(MPB) in buffered solution at neutral pH, a second band at 500 nm appeared (Fig. 7). By contrast, Fe^{II}(MPH) showed no absorbance band in that region of the spectrum, regardless of peroxide concentration (Fig. S25). Based on the following studies, we assign the species that forms upon treatment of Fe^{II}(MPB) under conditions of excess peroxide as Fe^{III}(MPP) (Scheme 2) and the band at 500 nm as a LMCT band for a phenolate complex. At 2 equivalents of peroxide in buffered solution, approximately 15% of the species is Fe^{III}(MPP), indicating that it is a minor component. However, the complex forms more readily in the absence of buffer, so further studies to identify this species were carried out in the absence of buffer.

To probe solution speciation under conditions of excess peroxide addition to Fe^{II}(MPB), high resolution mass spectrometry was performed on the product solutions at pH 7.4 (Fig. S44 to S47). These data show that with two equivalents of peroxide in solutions lacking buffer the phenolate complex Fe^{III}(MPP) is formed as a minor component (13% relative abundance). However, with ten equivalents of peroxide the Fe^{III}(MPP) complex is one of the most abundant species in solution. Complexes assigned as end-on (Fe^{III}(MPB)(OOH)) and side-on (Fe^{III}(MPB)(OO)) peroxo are identified as minor species (38% and 13% relative abundance) with respect to Fe^{III}(MPP). Notably, end-on and side on peroxide complexes of analogous Fe(III) complexes with five nitrogen donor groups form upon treatment with peroxide and with base.[49,62,68] The Fe(III) peroxo complex then may undergo heterolytic O–O cleavage to produce a high valent Fe(IV) oxo complex.[48,63] Such

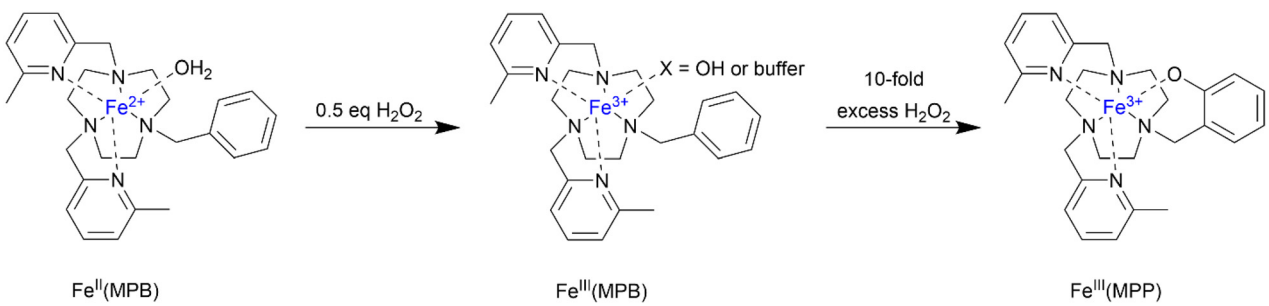

Scheme 2 Oxidation products.

high valent oxoiron(IV) complexes have been shown to oxidize non-coordinating benzyl groups to phenolate ligands.[69]

Further solution studies were carried out with Fe^{II}(MPB) and peroxide in solutions lacking buffer, conditions where Fe^{III}(MPP) more readily forms. UV-vis spectra are shown for Fe^{II}(MPB) treated with two equivalents of peroxide and titrated as a function of pH (Fig. S48). Under these conditions, the phenol complex Fe^{III}(MPP) is present as a major species as shown by the absorbance band at 500 nm at neutral to basic pH. As the pH becomes more acidic, a new band appears at 600 nm which is assigned to the LMCT band of the protonated Fe^{III}(MPP) complex. The intensity of this peak increases upon titration from pH 6.5 to pH 4.0 (Fig. S49). Plots of these data give an apparent pK_a value of 5.7 for the deprotonation of the phenol. In a second set of experiments, cyclic voltammetry studies of aqueous solutions of Fe^{II}(MPB) with KCl, no buffer and one equivalent of peroxide were studied (Fig. S50). A new quasi-reversible wave was observed at more negative values than the original complex with an $E_{1/2}$ of 375 mV. This species is assigned as a protonated phenol complex and is observed at acidic pH values (pH 4) in unbuffered solutions.

Probe characteristics

The water proton relaxivity of the Fe(II) complexes and their corresponding Fe(III) analogs were measured (Table S12) at 1.4 T and 34 °C on an NMR spectrometer and at 7.0 T and 37 °C on an MRI scanner. As anticipated, the Fe(II) complexes showed low relaxivities of 0.05 and 0.09 mM^{-1} s^{-1} respectively at 1.4 T. This low relaxivity is consistent with Fe(II) complexes being paramagnetic shift agents rather than relaxivity agents as highlighted by the NMR spectra in Fig. 2. The relaxivity increased by 14-fold and 7-fold respectively for Fe^{III}(MPB) and Fe^{III}(MPH) upon treatment with two equivalents of peroxide. Plots of R_1 as a function of iron complex (Fig. S52) gave relaxivities of 0.71 mM^{-1} s^{-1} and 0.86 $mM^{-1}s^{-1}$ for Fe^{III}(MPB) and 0.58 mM^{-1} s^{-1} and 0.63 $mM^{-1}s^{-1}$ for Fe^{III}(MPH), at 1.4 T and 7 T respectively (Table S12). Addition of serum albumin did not alter the relaxivity of Fe^{III}(MPB) but increased the relaxivity of Fe^{III}(MPH) slightly to 0.73 mM^{-1} s^{-1}. The relaxivity values for both complexes are characteristic of closed-coordinate Fe(III) high-spin complexes which function through second-sphere water interactions. This suggests that Fe^{III}(MPB) either has a slowly exchanging water ligand, or a hydroxide ligand. Relaxivity values tracked as a function of equivalents of peroxide added to Fe^{II}(MPB) showed a decrease at high peroxide conditions (>100), with nearly constant values from one equivalent to 50 equivalents of peroxide (Table S13). This is consistent with the initial formation of Fe^{III}(MPB) complex at low peroxide followed by the formation of the phenol complex at high concentrations of peroxide.

MRI phantoms (Fig. 8, S54 & S56) show that the R_1 and R_2 of the Fe^{II} complexes increase as a function of concentration and upon oxidation by peroxide. (Note that R_1 and R_2 are the rate constants associated with T_1 and T_2 processes.) The left side of the array corresponds to the Fe(II) complex and the right side of the array corresponds to the Fe(III) complex. The most highly concentrated Fe(III) sample shows the brightest contrast in both the maps. This is consistent with the enhancement of R_1 relaxation rate constant upon oxidation of the Fe(II) complexes to give rise to higher relaxivity Fe(III) species. A turn-on ratio of 11 and 7 for r_1 relaxivity of Fe^{III} to Fe^{II} is observed at 7 T for Fe^{II}(MPB) and Fe^{II}(MPH) respectively.

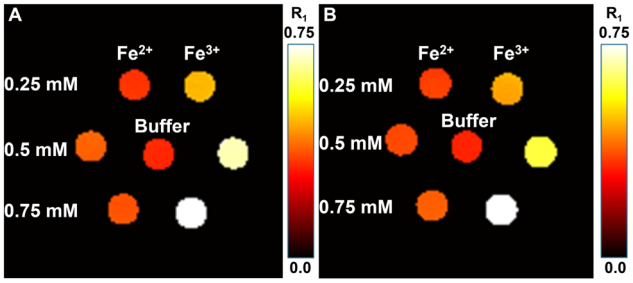

Fig. 8 R_1 (s^{-1}) map of Fe^{II}(MPB) (A) and Fe^{II}(MPH) (B) before and after oxidation. Conditions: 0 to 0.75 mM complex, 2 eq. H_2O_2, 20 mM HEPES pH 7.4, 0.1 M NaCl, 310 K, 7 T.

The reversibility of the response of the MRI probes towards oxidation and reduction was studied (Fig. 9). One equivalent of peroxide was added followed by addition of one equivalent of ascorbate to solutions containing 500 μM probe. After the first cycle, the relaxivity values were similar to the original $Fe^{(II)}$ values. However, the second oxidation produced slightly lower relaxivity values than the first oxidation. The lack of complete reversibility is attributed, in part, to the characteristics of probe solution chemistry over time. Notably, the relaxivity of Fe^{III}(MPB) and Fe^{III}(MPH) decreases slightly when monitored over several hours in the presence and absence of human serum albumin (Tables S15 & S16, Fig. S57 & 58). In the

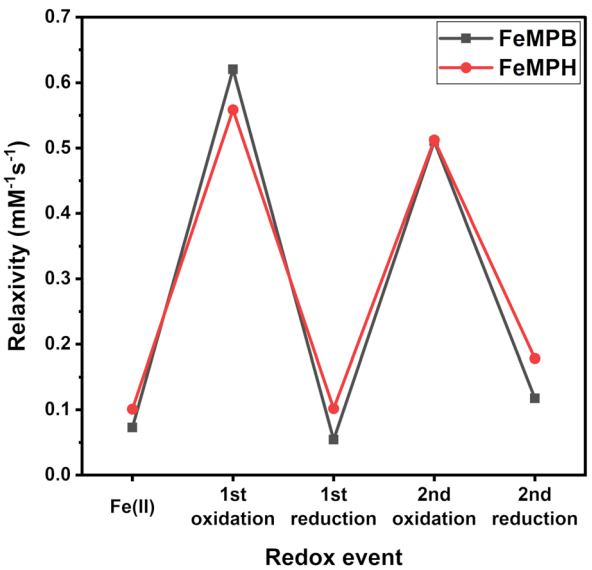

Fig. 9 Relaxivity of Fe^{II}(MPB) and Fe^{II}(MPH) complexes following cycles of oxidation and reduction with peroxide and ascorbate. Conditions: 20 mM HEPES pH 7.4, 0.1 M NaCl, 307 K, 0.50 mM complex, 0.50 mM H_2O_2, followed by 0.50 mM ascorbate.

absence of human serum albumin, the relaxivities of both the complexes decreased by 25 percent over four hours. In the presence of human serum albumin, Fe^{III}(MPB) decreased by 33% and Fe^{III}(MPH) decreased by 11%. Addition of an equivalent of peroxide partially restored the relaxivity of Fe^{III}(MPB), but not Fe^{III}(MPH) in solutions containing 500 μM complex at neutral pH (Fig. S59). UV-vis spectroscopy experiments (Fig. S60 and S61) at lower concentrations (200 μM) showed full restoration of electronic absorbance bands of Fe^{III}(MPB) and Fe^{III}(MPH), upon addition of half an equivalent of peroxide at 4 hours, suggesting that the complexes are slowly reduced in solution over several hours.

Conclusions

Consideration of the coordination chemistry of peroxide with Fe(II) complexes is instrumental in the design of a redox-responsive MRI probe that is selective for peroxide over O_2. Although the relatively high oxidation potential of the iron center (680 mV) indicates that outer-sphere oxidation by peroxide ($H_2O_2/OH^{\bullet -}$, $E^{\circ\prime}$ = 390 mV) should be unfavorable, exposure to one equivalent of peroxide nonetheless yields the Fe^{III}(MPB) complex, most likely through an inner-sphere redox processes. Oxidation is rapid, similar to other Fe(II) probes that contain available sites for inner-sphere oxidation with peroxide.[38] The rapid reaction of the Fe^{II}(MPH) complex with peroxide is consistent with the availability of a coordination site for binding an incoming ligand either through formation of a seven-coordinate complex or by displacement of the hydroxypropyl pendant as well as the lower redox potential of the probe. Moreover, the interaction of the hydroxypropyl group with peroxide has been proposed to increase the rate of oxidation, as shown for analogous Co(II) complexes.[70]

The selectivity of the Fe^{II}(MPB) probe for oxidation by peroxide over oxygen is promising and the turn-on ratio is similar to that of other iron-based probes.[38,40] However, improved overall relaxivity of the Fe(III) complex is desirable and may be accomplished by optimizing relaxivity parameters such as correlation times through larger assemblies and by modulation of water exchange[71] as well efforts towards improving water solubility.

Finally, the oxidation of the aromatic ring to a phenolate group might be prevented by addition of *ortho*-substituents[72] or the non-coordinating pendent may be changed to a less easily oxidized group. These modifications are underway towards rapid-response, high selectivity peroxide-responsive iron-based MRI probes.

Author contributions

DKB: investigation, analysis, validation, writing; JAS: investigation, data curation, software; MRC: investigation and analysis; JRM: conceptualization, writing, funding acquisition.

Conflicts of interest

JRM is the cofounder of Ferric Contrast, Inc., a company that develops iron-based contrast agents.

Data availability

The datasets supporting this article have been uploaded as part of the supplementary information (SI). Supplementary information: materials and methods, synthetic procedures, spectroscopic characterization, crystallographic data, NMR data, electrochemistry, MRI phantoms. See DOI: **https://doi.org/10.1039/d6qi00660d**.

Additional data will be provided by the authors upon reasonable request.

CCDC 2539019 contains the supplementary crystallographic data for this paper.[73]

Acknowledgements

JRM thanks the National Science Foundation (CHE-2400128) for support of this research. This work utilized a Rigaku XtaLAB Synergy-S diffractometer that was purchased with funding from NSF (CHE-2216151), and the Bruker 500 MHz NMR (NSF CHE-2018160), ICP-MS and FTMS (NSF CHE-0959565). JAS is grateful for the Roswell Park's Comprehensive Cancer Center Support Grant: P30CA016056. The 7T MRI scanner was purchased through funds from NIH award S10OD030397.

References

1 J. Wahsner, E. M. Gale, A. Rodriguez-Rodriguez and P. Caravan, Chemistry of MRI Contrast Agents: Current Challenges and New Frontiers, *Chem. Rev.*, 2019, **119**, 957–1057.
2 C. Westbrook and J. Talbot, *MRI in Practice*, Wiley-Blackwell, Hoboken, NJ, 5th edn, 2018.
3 S. Shuvaev, E. Akam and P. Caravan, Molecular MR Contrast Agents, *Invest. Radiol.*, 2021, **56**, 20–34.
4 L. M. De Leon-Rodriguez, A. J. Lubag, C. R. Malloy, G. V. Martinez, R. J. Gillies and A. D. Sherry, Responsive MRI agents for sensing metabolism in vivo, *Acc. Chem. Res.*, 2009, **42**, 948–957.
5 H. Li and T. J. Meade, Molecular magnetic resonance imaging with Gd(III)-based contrast agents: challenges and key advances, *J. Am. Chem. Soc.*, 2019, **141**, 17025–17041.
6 S. M. Pinto, V. Tome, M. J. F. Calvete, M. M. C. A. Castro, E. Toth and C. F. G. C. Geraldes, Metal-based redox-responsive MRI contrast agents, *Coord. Chem. Rev.*, 2019, **390**, 1–31.
7 S. S. Xue, Y. Pan, W. Pan, S. Liu, N. Li and B. Tang, Bioimaging agents based on redox-active transition metal complexes, *Chem. Sci.*, 2022, **13**, 9468–9484.

8 J. R. Morrow, J. J. Raymond, M. S. I. Chowdhury and P. R. Sahoo, Redox-Responsive MRI Probes Based on First-Row Transition-Metal Complexes, *Inorg. Chem.*, 2022, **61**, 14487–14499.
9 C. S. Bonnet and E. Toth, Metal-based environment-sensitive MRI contrast agents, *Curr. Opin. Chem. Biol.*, 2021, **61**, 154–169.
10 P. Yue and G. Angelovski, How to Develop Bioresponsive MRI Probes Based on Paramagnetic Gd(III) for Applications, *Anal. Sens.*, 2023, **3**, 2629–2742.
11 S. Karbalaei and C. R. Goldsmith, Recent advances in the preclinical development of responsive MRI contrast agents capable of detecting hydrogen peroxide, *J. Inorg. Biochem.*, 2022, **230**, 111763.
12 J. D. Hayes, A. T. Dinkova-Kostova and K. D. Tew, Oxidative Stress in Cancer, *Cancer Cell*, 2020, **38**, 167–197.
13 M. Mittal, M. R. Siddiqui, K. Tran, S. P. Reddy and A. B. Malik, Reactive Oxygen Species in Inflammation and Tissue Injury, *Antioxid. Redox Signaling*, 2014, **20**, 1126–1167.
14 C. Nathan and A. Cunningham-Bussel, Beyond oxidative stress: an immunologist's guide to reactive oxygen species, *Nat. Rev. Immunol.*, 2013, **13**, 349–361.
15 A. El-Kenawi and B. Ruffell, Inflammation, ROS, and Mutagenesis, *Cancer Cell*, 2017, **32**, 727–729.
16 M. Abdesselem, N. Pétri, R. Kuhner, F. Mousseau, V. Rouffiac, T. Gacoin, C. Laplace-Builhé, A. Alexandrou and C. I. Bouzigues, Real-time in vivo ROS monitoring with luminescent nanoparticles reveals skin inflammation dynamics, *Biomed. Opt. Express*, 2023, **14**, 5392–5404.
17 W. H. Yu, Y. M. Tu, Z. Long, J. Z. Liu, D. Q. Kong, J. Peng, H. Wu, G. Zheng, J. Z. Zhao, Y. H. Chen, R. Liu, W. L. Li and C. X. Hai, Reactive Oxygen Species Bridge the Gap between Chronic Inflammation and Tumor Development, *Oxid. Med. Cell. Longevity*, 2022, **2022**, 2606928.
18 H. Sies, V. V. Belousov, N. S. Chandel, M. J. Davies, D. P. Jones, G. E. Mann, M. P. Murphy, M. Yamamoto and C. Winterbourn, Defining roles of specific reactive oxygen species (ROS) in cell biology and physiology, *Nat. Rev. Mol. Cell Biol.*, 2022, **23**, 499–515.
19 Y. Feng, C. Santoriello, M. Mione, A. Hurlstone and P. Martin, Live Imaging of Innate Immune Cell Sensing of Transformed Cells in Zebrafish Larvae: Parallels between Tumor Initiation and Wound Inflammation, *PLos Biol.*, 2010, **14**, e1002377.
20 W. H. Koppenol and R. H. Hider, Iron and redox cycling. Do's and don'ts, *Free Radical Biol. Med.*, 2019, **133**, 3–10.
21 P. B. Tsitovich, P. J. Burns, A. M. Mckay and J. R. Morrow, Redox-activated MRI contrast agents based on lanthanide and transition metal ions, *J. Inorg. Biochem.*, 2014, **133**, 143–154.
22 Q. N. Do, J. S. Ratnakar, Z. Kovacs and A. D. Sherry, Redox- and Hypoxia-Responsive MRI Contrast Agents, *ChemMedChem*, 2014, **9**, 1116–1129.
23 A. Li, X. X. Tang, X. Q. Gong, H. M. Chen, H. Y. Lin and J. H. Gao, A fluorinated bihydrazide conjugate for activatable sensing and imaging of hypochlorous acid by 19-F NMR/MRI, *Chem. Commun.*, 2019, **55**, 12455–12458.
24 Y.-X. Chen, A. Ge, X. Guo, M. Yu and J. Tao, Spin State Modulation Strategies for Transition Metal-Based MRI Contrast Agents, *Chem. Biomed. Imaging*, 2026, **4**, 274–303.
25 E. C. Lewandowski, C. B. Arban, M. P. Deal, A. L. Batchev and M. J. Allen, Europium(II/III) coordination chemistry toward applications, *Chem. Commun.*, 2024, **60**, 10655–10671.
26 L. A. Basal and M. J. Allen, Synthesis, Characterization, and Handling of Eu Containing Complexes for Molecular Imaging Applications, *Front. Chem.*, 2018, **6**, 65.
27 S. A. A. S. Subasinghe, C. J. Ortiz, J. Romero, C. L. Ward, A. G. Sertage, L. Kurenbekova, J. T. Yustein, R. G. Pautler and M. J. Allen, Toward quantification of hypoxia using fluorinated EuII/III-containing ratiometric probes, *Proc. Natl. Acad. Sci. U. S. A.*, 2023, **120**(15), e2220891120.
28 S. M. A. Pinto, A. R. R. Ferreira, D. S. S. Teixeira, S. C. C. Nunes, A. L. M. Batista de Carvalho, J. M. S. Almeida, Z. Garda, A. Pallier, A. A. C. C. Pais, C. M. A. Brett, E. Toth, M. P. M. Marques, M. M. Pereira and C. F. G. C. Geraldes, Fluorinated Mn(III)/(II)-Porphyrin with Redox-Responsive (1) H and (19) F Relaxation Properties, *Chem. – Eur. J.*, 2023, **29**, e202301442.
29 D. Xie, M. Yu, R. T. Kadakia and E. L. Que, F-19 Magnetic Resonance Activity-Based Sensing Using Paramagnetic Metals, *Acc. Chem. Res.*, 2020, **53**, 2–10.
30 P. B. Tsitovich, J. A. Spernyak and J. R. Morrow, A redox-activated MRI contrast agent that switches between paramagnetic and diamagnetic states, *Angew. Chem., Int. Ed.*, 2013, **52**, 13997–14000.
31 A. M. Funk, V. C. Jordan, A. D. Sherry, S. J. Ratnakar and Z. Kovacs, Oxidative Conversion of a Europium(II)-Based T-1 Agent into a Europium(III)-Based paraCEST Agent that can be Detected In Vivo by Magnetic Resonance Imaging, *Angew. Chem., Int. Ed.*, 2016, **55**, 5024–5027.
32 E. A. Kras, E. M. Snyder, G. E. Sokolow and J. R. Morrow, Distinct Coordination Chemistry of Fe(III)-Based MRI Probes, *Acc. Chem. Res.*, 2022, **55**, 1435–1444.
33 J. R. Morrow and J. J. Raymond, in *Metal ions in life sciences (Lanthanides and Other Transition Metal Ion Complexes and Nanoparticles in Magnetic Resonance Imaging), Metal Ions in Life Sciences 27*, ed. C. F. G. C. Geraldes, A. Sigel, H. Sigel, E. Fresinger and R. K. O. Sigel, Taylor & Francis, 2023.
34 A. Gupta, P. Caravan, W. S. Price, C. Platas-Iglesias and E. M. Gale, Applications for transition-metal chemistry in contrast-enhanced magnetic resonance imaging, *Inorg. Chem.*, 2020, **59**, 6648–6678.
35 Z. Baranyai, F. Carniato, A. Nucera, D. Horvath, L. Tei, C. Platas-Iglesias and M. Botta, Defining the conditions for the development of the emerging class of Fe(III)-based MRI contrast agents, *Chem. Sci.*, 2021, **12**, 11138.
36 N. Kuznik and M. Wyskocka, Iron(III) Contrast Agent Candidates for MRI: a Survey of the Structure-Effect Relationship in the Last 15 Years of Studies, *Eur. J. Inorg. Chem.*, 2016, **4**, 445–458.

37 P. B. Tsitovich, F. Gendron, A. Y. Nazarenko, B. N. Livesay, A. P. Lopez, M. P. Shores, J. Autschbach and J. R. Morrow, Low-Spin Fe(III) Macrocyclic Complexes of Imidazole-Appended 1,4,7-Triazacyclononane as Paramagnetic Probes, *Inorg. Chem.*, 2018, **57**, 8364–8374.

38 H. Wang, V. C. Jordan, I. A. Ramsay, M. Sojoodi, B. C. Fuchs, K. K. Tanabe, P. Caravan and E. M. Gale, Molecular magnetic resonance imaging using a redox-active iron complex, *J. Am. Chem. Soc.*, 2019, **141**, 5916–5925.

39 R. T. Kadakia, R. T. Ryan, D. J. Cooke and E. L. Que, An Fe complex for (19)F magnetic resonance-based reversible redox sensing and multicolor imaging, *Chem. Sci.*, 2023, **14**, 5099–5105.

40 S. Karbalaei, A. Franke, A. Jordan, C. Rose, P. R. Pokkuluri, R. J. Beyers, A. Zahl, I. Ivanovic-Burmazovic and C. R. Goldsmith, A Highly Water- and Air-Stable Iron-Containing MRI Contrast Agent Sensor for H_2O_2, *Chem. – Eur. J.*, 2022, **28**, e202201179.

41 S. Karbalaei, A. Franke, A. Zahl, P. R. Pokkuluri, R. J. Beyers, I. Ivanovic-Burmazovic and C. R. Goldsmith, An Fe(ii) complex detects hydrogen peroxide with ^{1}H and ^{19}F magnetic resonance imaging responses, *Chem. Commun.*, 2025, **61**, 15898–15901.

42 A. A. Kitos, R. Castañeda, Z. J. Comeau, N. Mavragani, N. D. Calvert, A. Kirby, F. M. Martinez-Santiesteban, P. J. Pallister, T. J. Scholl, M. Murugesu, A. J. Shuhendler and J. L. Brusso, Cluster-based redox-responsive super-atomic MRI contrast agents, *Chem*, 2025, **11**, 102330.

43 K. K. Huang, M. M. Li, X. Zhang, X. Linghu, Y. B. Wang, W. C. Li, P. J. Wu, J. Q. Dong, S. P. Yang and J. J. Jiao, Magnetically switchable coordination cages: a class of supramolecular contrast agents for tumor-responsive magnetic resonance imaging, *Sci. China. Chem.*, 2026, DOI: 10.1007/s11426-025-3181-8.

44 Z. Garda, F. Szeremeta, C. N. Tóth, S. Bunda, C. Pifferi, R. Clémençon, S. Même, G. Tircsó and É. Tóth, Relaxation-Based In Vivo Discrimination of Oxidized and Reduced States of a Redox-Switchable ^{19}F MRI Probe, *J. Am. Chem. Soc.*, 2025, **147**, 18017–18024.

45 V. C. Jordan, M. Sojoodi, S. Shroff, P. G. Pagan, S. C. Barrett, J. Wellen, K. K. Tanabe, R. T. Chung, P. Caravan and E. M. Gale, Molecular magnetic resonance imaging of liver inflammation using an oxidatively activated probe, *JHEP Rep.*, 2023, **5**(10), 100850.

46 R. M. King, M. J. Gounis, E. J. Schmidt, A. Leporati, E. M. Gale and A. J. r. Bogdanov, Molecular Magnetic Resonance Imaging of Aneurysmal Inflammation Using a Redox Active Iron Complex, *Invest. Radiol.*, 2023, **58**, 656–662.

47 I. A. Rosales, I. Y. Zhou, I. Ay, M. Sojoodi, M. E. Sise and E. M. Gale, Imaging kidney inflammation using an oxidatively activated MRI probe, *Kidney Int.*, 2024, **106**, 671–678.

48 J. Chen, A. S. Sardjan, C. M. de Roo, M. Di Berto Mancini, A. Draksharapu, D. Angelone, R. Hage, M. Swart and W. R. Browne, Generation of $[(N4Py)Fe(IV)=O]^{2+}$ through Heterolytic O-O Bond Cleavage in [(N4Py)Fe(II)(OOH)], *Inorg. Chem.*, 2025, **64**, 9408–9417.

49 G. Roelfes, V. Vrajmasu, K. Chen, R. Y. Ho, J. U. Rohde, C. Zondervan, R. M. La Crois, E. P. Schudde, M. Lutz, A. L. Spek, R. Hage, B. L. Feringa, E. Munck and L. Que Jr., End-on and side-on peroxo derivatives of non-heme iron complexes with pentadentate ligands: models for putative intermediates in biological iron/dioxygen chemistry, *Inorg. Chem.*, 2003, **42**, 2639–2653.

50 X. P. Zhang, D. L. Zhang, D. H. Busch and R. van Eldik, Catalytic action of the iron(II) complexes of 8-methyl-1,4-bis(2-pyridylmethyl)-1,4,8-triazacycloundecane and 1-methyl-5,9-bis(2-pyridylmethyl)-1,5,9 triazacyclododecane, *J. Chem. Soc., Dalton Trans.*, 1999, 2751–2758.

51 P. B. Tsitovich, J. M. Cox, J. B. Benedict and J. R. Morrow, Six-coordinate Iron(II) and Cobalt(II) paraSHIFT Agents for Measuring Temperature by Magnetic Resonance Spectroscopy, *Inorg. Chem.*, 2016, **55**, 700–716.

52 J. Wang, C. Gondrand, F. Touti and J. Hasserodt, A pair of highly biotolerated diamagnetic and paramagnetic iron(II) complexes displaying electroneutrality, *Dalton Trans.*, 2015, **44**, 15391–15395.

53 J. Salaam, T. Fogeron, G. Pilet, R. Bolbos, C. Bucher, L. Khrouz and J. Hasserodt, Unprecedented Relaxivity Gap in pH-Responsive Fe(III) -Based MRI Probes, *Angew. Chem., Int. Ed.*, 2023, **62**, e202212782.

54 L. Christiansen, D. N. Hendrickson, H. Toftlund, S. R. Wilson and C. L. Xie, Synthesis and Structure of Metal-Complexes of Triaza Macrocycles with 3 Pendant Pyridylmethyl Arms, *Inorg. Chem.*, 1986, **25**, 2813–2818.

55 P. B. Tsitovich, T. Y. Tittiris, J. M. Cox, J. B. Benedict and J. R. Morrow, Fe(II) and Co(II) methylated CYCLEN complexes as paraSHIFT agents with large temperature dependent shifts, *Dalton Trans.*, 2018, **47**, 916–924.

56 E. M. Snyder, D. Asik, S. M. Abozeid, A. Burgio, G. Bateman, S. G. Turowski, J. A. Spernyak and J. R. Morrow, A Class of FeIII Macrocyclic Complexes with Alcohol Donor Groups as Effective T_1 MRI Contrast Agents, *Angew. Chem.*, 2020, **132**, 2435–2440.

57 A. Brausam, J. Maigut, R. Meier, P. A. Szilágyi, H.-J. r. Buschmann, W. Massa, Z. Homonnay and R. van Eldik, Detailed spectroscopic, thermodynamic, and kinetic studies on the protolytic equilibria of FeIII(cydta) and the activation of hydrogen peroxide, *Inorg. Chem.*, 2009, **48**, 7864–7884.

58 J. Maigut, R. Meier, A. Zahl and R. van Eldik, Elucidation of the solution structure and water-exchange mechanism of paramagnetic [Fe (edta)(HO)], *Inorg. Chem.*, 2007, **46**, 5361–5371.

59 J. Maigut, R. Meier, A. Zahl and R. van Eldik, Effect of chelate dynamics on water exchange reactions of paramagnetic aminopolycarboxylate complexes, *Inorg. Chem.*, 2008, **47**, 5702–5719.

60 J. Maigut, R. Meier, A. Zahl and R. van Eldik, Triggering Water Exchange Mechanisms via Chelate Architecture. Shielding of Transition Metal Centers by

Aminopolycarboxylate Spectator Ligands, *J. Am. Chem. Soc.*, 2008, **130**, 14556–14569.

61 N. Elgrishi, K. J. Rountree, B. D. McCarthy, E. S. Rountree, T. T. Eisenhart and J. L. Dempsey, A Practical Beginner's Guide to Cyclic Voltammetry, *J. Chem. Educ.*, 2018, **95**, 197–206.

62 A. Bohn, C. Chinaux-Chaix, K. Cheaib, R. Guillot, C. Herrero, K. Senechal-David, J. N. Rebilly and F. Banse, Base-controlled mechanistic divergence between iron(iv)-oxo and iron(iii)-hydroperoxo in the H_2O_2 activation by a nonheme iron(ii) complex, *Dalton Trans.*, 2019, **48**, 17045–17051.

63 F. F. Li, J. England and L. Que, Near-Stoichiometric Conversion of H_2O_2 to Fe(IV)=O at a Nonheme Iron(II) Center. Insights into the O-O Bond Cleavage Step, *J. Am. Chem. Soc.*, 2010, **132**, 2134–2135.

64 H. J. Forman, A. Bernardo and K. J. A. Davies, What is the concentration of hydrogen peroxide in blood and plasma?, *Arch. Biochem. Biophys.*, 2016, **603**, 48–53.

65 F. I. Adam, P. L. Bounds, R. Kissner and W. H. Koppenol, Redox Properties and Activity of Iron-Citrate Complexes: Evidence for Redox Cycling, *Chem. Res. Toxicol.*, 2015, **28**, 604–614.

66 D. Asik, R. Smolinski, S. M. Abozeid, T. B. Mitchell, S. G. Turowski, J. A. Spernyak and J. R. Morrow, Modulating the properties of Fe(III) macrocyclic MRI contrast agents by appending sulfonate or hydroxyl groups, *Molecules*, 2020, **25**, 2291.

67 D. Asik, S. M. Abozeid, S. G. Turowski, J. A. Spernyak and J. R. Morrow, Dinuclear Fe(III) Hydroxypropyl-Appended Macrocyclic Complexes as MRI Probes, *Inorg. Chem.*, 2021, **60**, 8651–8664.

68 K. B. Jensen, C. J. McKenzie, L. P. Nielsen, J. Z. Pedersen and H. M. Svendsen, Deprotonation of low-spin mononuclear iron(III)-hydroperoxide complexes give transient blue species assigned to high-spin iron(III)-peroxide complexes, *Chem. Commun.*, 1999, 1313–1314.

69 Y. Sheng, C. S. Abelson, J. Prakash, A. Draksharapu, V. Young and L. Que, Unmasking Steps in Intramolecular Aromatic Hydroxylation by a Synthetic Nonheme Oxoiron (IV) Complex, *Angew. Chem., Int. Ed.*, 2021, **60**, 20991–20998.

70 K. M. Scott, B. L. Davenport, S. Vasylevskyi and E. L. Que, Improved Redox-Responsive Cobalt(II) ^{19}F Magnetic Resonance Imaging Agents through Addition of Hydrogen Bond Donors, *Inorg. Chem.*, 2025, **64**, 11130–11138.

71 L. Palagi, D. L. Longo, E. Toth, C. C. Quattrocchi, A. J. van der Molen, S. Aime and E. Gianolio, Molecular and supramolecular routes to enhance Gadolinium-based contrast agents relaxivity: How far are we from the theoretical optimalvalue?, *Eur. J. Med. Chem.*, 2025, **292**, 117668.

72 N. Pal, J. Xiong, M. Jahja, S. Mahri, V. J. r. Young, Y. S. Guo, M. Swart and L. J. r. Que, A 5,000-fold increase in the HAT reactivity of a nonheme Fe=O complex simply by replacing two pyridines of the pentadentate N4Py ligand with pyrazoles, *Proc. Natl. Acad. Sci. U. S. A.*, 2025, **122**, e2414962122.

73 CCDC 2539019: Experimental Crystal Structure Determination, 2026, DOI: **10.5517/ccdc.csd.cc2r71vx**.

